Fabrication and Characterization of

Carbon Nanotube Field-Effect Transistor Biosensors

Matthew R. Leyden, Canan Schuman, Tal Sharf, Josh Kevek, Vincent T. Remcho, Ethan D. Minot
Dept. of Physics, Oregon State University, Corvallis, OR, USA 97331;

ABSTRACT

We report the fabrication of carbon nanotube field-effect transistors for biosensing applications and the development of protocols for reliable protein and DNA sensing. The sensing method we employ is 'label free', relying only on the intrinsic charge of the biological molecule of interest. We discuss fabrication issues that we have solved, for example the preparation of clean surfaces, and the sensing protocol issues that we have encountered. Polylysine and ss-dna, highly charged biological molecules, are used as model systems to illustrate the performance of our biosensors.

Keywords: Label-free biosensor, Biosensor, Carbon nanotube, Nanoelectronics, Protein sensor, Mass-transport, Microfluidics.

1. INTRODUCTION

Over the last decade, a variety of protein and DNA sensors have been developed that circumvent the need for fluorescent labeling and fluorescence imaging.[1-6] Development of these label-free detection schemes is motivated by the need for faster, lower-cost detection of biomolecules. By removing the need for labeling and imaging, researchers hope to make biosensors more accessible to doctors and patients. This access to quantitative information about the presence of specific biomolecules in a patient's body is a critical step towards more accurate and personalized medical care.[7]

To detect unlabeled biomolecules, label-free detection schemes utilize intrinsic protein properties such as polarizability, mass and electric charge. Surface plasmon resonance,[1] optical waveguides[2] and impedance sensors[3] rely on the dielectric constant of biomolecules. The mass of biomolecules creates a signal for sensors based on micromechanical oscillators.[4] Charged biomolecules can be detected by nanowire field effect transistors (FETs)[5] and carbon nanotube (CNT) FETs.[6] In the class of charge-sensitive biosensors, semiconducting CNTs are extremely promising. Carbon nanotubes are hollow cylinders of sp^2 bonded carbon with a typical diameter of 1-2 nm. All atoms of the CNT are on the surface, carrier mobility is exceptionally high, and the sp^2 bonded carbon lattice is extremely stable in biological environments.

Figure 1 illustrates the basic transduction mechanism of a CNT FET biosensor. The conductance G of the semiconducting CNT can be tuned either by ions in the liquid environment (Fig. 1a) or, equivalently, charged proteins binding to the CNT surface (Fig. 1b). Free carriers in the CNT are capacitively coupled to charges in the environment, therefore, the number of free carriers is extremely sensitive to charges in the environment. Conductance of the semiconducting CNT is proportional to the number of free carriers. Protein binding can have additional effects on the conductance of a CNT FET device. These additional effects have been the subject of detailed investigations.[8]
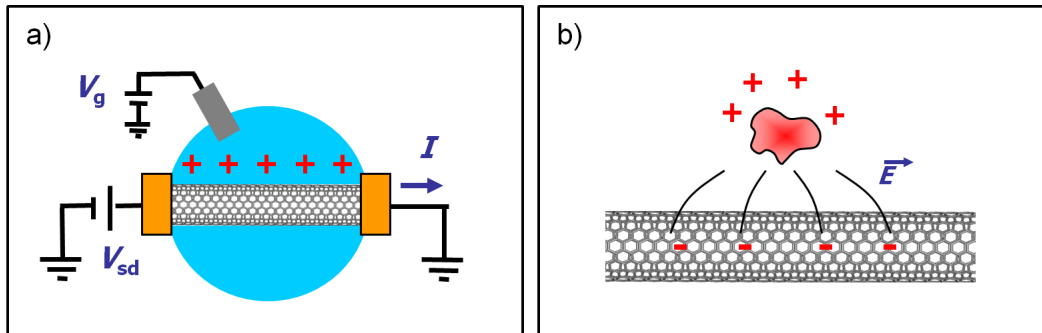
Figure 1. Gating of CNT field effect transistors. a) A semiconducting CNT is contacted by two metal electrodes (yellow). The gate voltage V_g sets the electrostatic potential of the buffer solution (blue). The gate voltage is applied using a Ag/AgCl reference electrode. Ions that condense on the CNT surface (shown as + symbols) induce carriers of the opposite charge in the CNT. b) A positively charge protein will also induce carriers of the opposite in the CNT.

Figure 2 shows data from a p-type CNT-FET biosensor. The free-carriers in the CNT are holes; the free-carriers are repelled by positive ions or positive proteins. Depletion of free carriers causes a decrease in the conductance of the sensor. In Figure 2a, conductance is tuned by changing the electrostatic potential V_g of the electrolyte solution that surrounds the sensor. In Figure 2b, the conductance changes due to proteins binding on the surface of the sensor. The total conductance change caused by protein binding can be expressed as an equivalent change in V_g. In Fig 2b, the binding of polylysine is equivalent to a shift $\Delta V_g = +55$ mV.

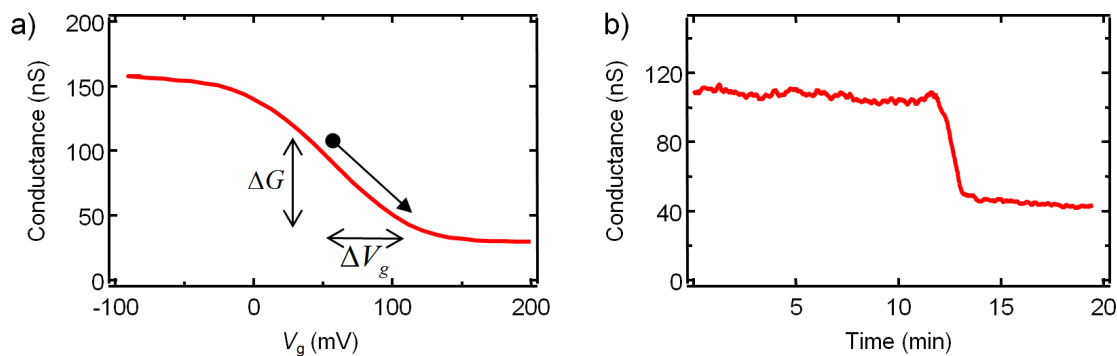

Figure 2. Measurements from a p-type CNT-FET biosensor. a) Transistor curve (conductance vs. V_g) of sensor gated by an electrolyte solution. ΔG and ΔV_g illustrate the effect of polylysine absorption. b) Real time sensing data with V_g set to 50 mV. Polylysine (MW110kD) 10 μg/ml in phosphate buffered saline is injected at 12 minutes. A flow rate of 3 ml/hr is maintained throughout the experiment.

While CNT FETs are among the most promising devices for label-free biosensing, researchers continue to wrestle with issues such as unknown noise sources, manufacturing reliability, spurious signals, and slow detection speed. In this contribution we describe the methods that we have developed for device manufacturing and controlling the sensing environment to avoid spurious signals. Using these methods, we have characterized detection speed and confirmed theoretical predictions of protein mass-transport.

2. CIRCUIT FABRICATION

2.1 Overview

Many fabrication processes have been developed for nanotube transistors.[9-11] These transistor devices can be broadly classified as (i) individual CNT devices and (ii) CNT network devices. Individual CNTs circuits are commonly

fabricated by patterning nanotube catalyst onto the device substrate and then growing CNTs directly on the device using catalyzed chemical vapor deposition (CVD).[9] This method relies on Poissonian statistics to randomly produce devices with zero, one or two CNTs (only a fraction of devices will have an individual CNT). Nanotube network devices typically involve fewer fabrication steps and higher yields of working devices. [10,11] However, these network devices do not give researchers insight into transduction mechanisms at the single CNT level. Moreover, individual CNT sensors are more promising than network sensors for single molecule sensing applications.
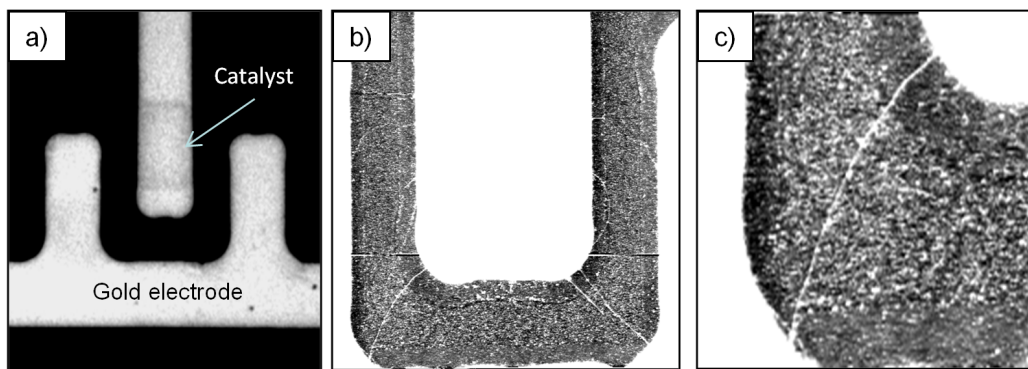

Figure 3. Nanotube Circuit. The electrodes have a width of 10μm a) Optical microscope image of a nanotube transistor. b) AFM image of a CNT transistor showing CNTs forming complete circuits. c) AFM of an individual CNT. Height range is 0 (black) to 2.5nm and above (white).

2.2 Fabrication of Individual CNT circuits

The CNT transistors used in the current experiments are created on silicon wafers that are p-doped and have a 300 nm top-surface oxide (Silicon Quest). An example of a finished device is shown in Figure 3. Before nanotube growth, alignment markers are patterned onto the chip using photolithography as shown in Figure 4a-c. The photoresist (S1813 from Microchem) is spun to nominal thickness 1.3 μm and patterned using a contact aligner (Karl Suss). After development, the photoresist is hardbaked (5 min at 115C) to prepare the resist for an oxide etch. Alignment markers are etched into the SiO_2 using buffered HF (20:1 buffer to HF ratio, total etch depth 100 nm).
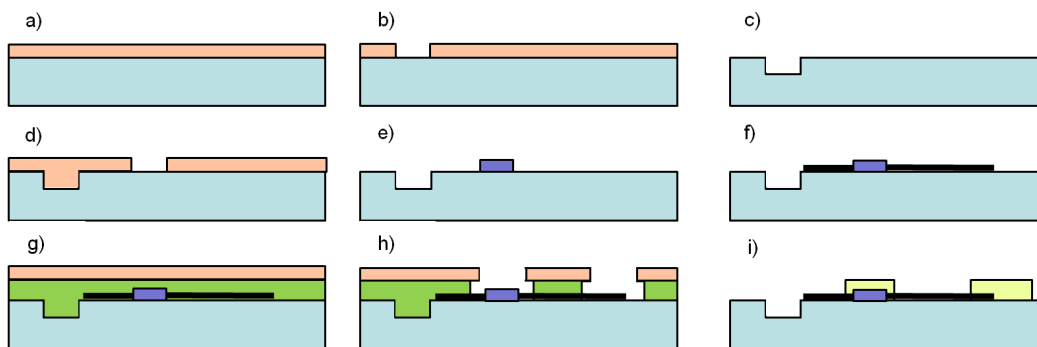

Figure 4. The biosensor device fabrication process. a) Photoresist is spun onto a silicon wafer. b) Photoresist is soft-baked, exposed, and developed, and hard-baked. c) The oxide is etched and the photoresist is removed. d) The wafer is patterned with photoresist and preparing for catalyst deposition. e) Catalyst is deposited onto the wafer and the photoresist is removed. f) Nanotubes are grown by CVD. g) Bilayer photoresist is spun onto the wafer. h) The photoresist is patterned and ready for metal evaporation. i) Cr/Au is thermally evaporated onto the wafer.

To selectively deposit catalyst on the chip (Figure 4d-e), a second photolithography step is performed. A wafer with patterned photoresist (S1813) is then exposed to catalyst by either drop casting a catalyst solution,[9] spinning on a catalyst

solution,[12] or electron-beam evaporation of a thin metal layer.[10] All three catalysts produce good results and differences between the methods are currently under investigation. The drop-cast catalyst solution is alumina supported CNT catalyst dissolved in DI water and has 1.3 mg/ml iron nitrate $Fe(NO_3)_3$, 0.3 mg/ml Molybdenum (VI) dioxide bis(acetyl-acetonate), and 1 mg/ml of nano-powdered alumina (Al_2O_3 from Degussa). The spun-on catalyst solution has 1mg/ml PVP (polyvinylpyrrrolidone MW 360 kDa) (Sigma Aldrich), 1mM iron nitrate (Sigma-Aldrich), and 0.5mM Molybdenum (VI) dioxide bis(acetyl-acetonate) (Strem Chemicals). The PVP increases the viscosity of the solution to give a uniform spin coat. Electron beam evaporated catalyst is pure iron and 0.2nm thick. Once the catalyst has been deposited, the photoresist is removed by rinsing sequentially with acetone, isopropyl alcohol, and DI water. Small rectangles of catalyst (6x10um) are left behind.

Catalyzed CVD growth of nanotubes is performed in a one-inch tube furnace using growth parameters based on an existing recipe.[13] Wafers are diced into 2x2 cm sections (small enough to fit in the one-inch tube furnace) and annealed in open air at 750 °C for 5 min. The furnace is then sealed, flushed with argon, and annealed with H_2 at 0.45 SLM for 10 min to remove oxygen from the metal catalyst. The furnace is flushed again with argon and ramped up to the nanotube growth stage at 900C. The gases during growth are 0.45 SLM H_2, 0.15 SLM Ar bubbled through ethanol, and 0.3 SLM Ar bubbled through methanol. The growth time is 15 min. The furnace is then cooled under an Ar flow. This growth technique produces CNTs with a range of diameters, from 1-3 nm.

The last step of circuit fabrication is the deposition of metal electrodes (Figure 4g-i). The chip is coated with a bi-layer photoresist (LOR3B and S1813 from Microchem). The under-layer (LOR3B) ensures an undercut profile which aids in metal lift off. After patterning the photoresist, the chip is placed in a thermal evaporator. The electrodes metals are Cr/Au (5 nm/30 nm) with the Cr layer promoting adhesion of the Au to the oxide surface. The evaporation rate is 1 A/s and residual gas pressure is $7x10^{-6}$ Torr or lower. After the metal deposition, photoresist and excess metal is lifted off by soaking in remover (Remover PG from Microchem) at 60°C for 1 hour. The chip is rinsed sequentially with acetone, isopropyl alcohol, and DI water before drying.

The photoresist used during fabrication leaves organic residues on the circuit. An effective way to clean the circuit before a biosensing experiment is to anneal for 10 minutes at 400°C in an Ar atmosphere (1 SLM Ar in a one-inch tube furnace).[14] Previous authors have noted the importance of this step before selective functionalizing of CNT can be achieved (section 4).[15] The annealing step affects the device properties, often increasing the contact resistance between the metal and the CNT. This may be due to oxidation of the Cr sticking layer and is currently under investigation.
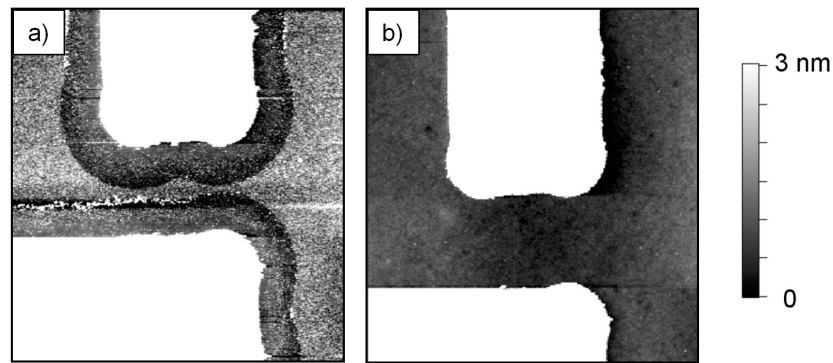

Figure 5. AFM images showing the effectiveness of surface cleaning. a) Metal electrodes (white) and the oxide surface directly after lift off. The electrodes are 10 μm wide. b) The same area after a 10 minute anneal in 1 SLM Ar at 400°C. The height scales for both images are identical. There is no CNT in this test circuit.

3. MICROFLUIDICS

3.1 Fluid delivery to the biosensor chip

Microfluidic channels made from polydimethylsiloxane (PDMS) are a well established method to deliver small volumes of solution to the active area of a biosensor.[16] PDMS channels can form temporary or permanent seals to silicon wafers and have potential for "lab on a chip" applications.
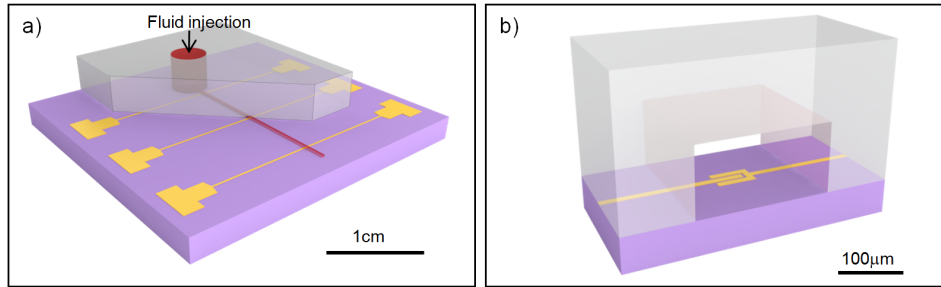

Figure 6. a) Cross section of a PDMS channel (gray) on our CNT FET biosensor chip (purple). Fluid is colored red for clarity. b) Magnified image showing the gap between electrodes and the width of the microfluidic channel.

The mold for creating a PDMS flow channel is made from 100 μm thick photoresist (SU8 3050 from Microchem). The photoresist mold is patterned in a contact aligner and then developed following the manufacturer's guidelines. PDMS is mixed (10:1 ratio of resin to hardener) and then poured on top of the photoresist mold. The PDMS is cured overnight at room temperature and then removed from the mold. The resulting flow channels are 100 μm tall and 200 μm wide.

The PDMS channel is pressed onto a CNT FET biosensor chip to form a water-tight seal with the oxide surface. We use a home-built acrylic fixture to clamp the PDMS in place. The fixture connects to inlet and outlet tubing (Teflon tubing, 0.009in inner diameter, Upchurch Scientific) and holds a Ag/AgCl reference electrode (model MF-2078, BAS) in contact with the solution in the channel. On the nanotube chip there is a gold working electrode which is used to gate the solution. The reference electrode is used to measure V_g. For small gating voltages (a small voltage produces under 1nA of faradaic current) the reference electrode can be used as both the working electrode and reference electrode with minimal error.[17]

3.2 Sensor response time and calibration

When delivering solution to the sensor, the lead volume must be flushed. The lead volume is the space in between the new solution and the sensor. A pH detection experiment was designed to find the lag time to reach fully-developed flow after solutions are switched (see Fig 7).
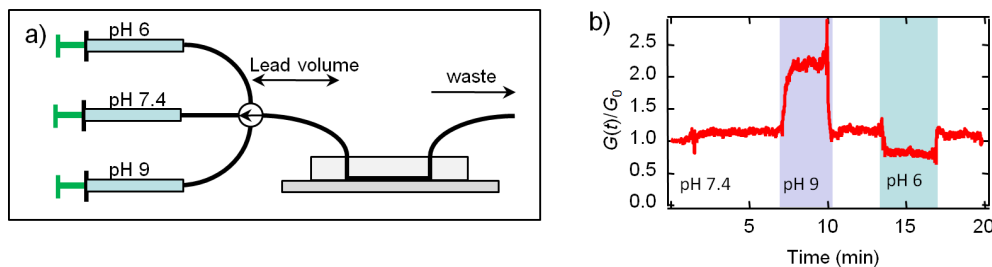

Figure 7. pH calibration on a nanotube circuit. a) Diagram of our microfluidic system showing 3 syringes with solutions of PBS at differing pH. A microfluidic hub (Upchurch Scientific, dead volume 12 μl) switches between different syringes. The lead volume of tubing is 6μl (15 cm length, 225 μm inner diameter) and lead volume in the PDMS is 6μl. b) Plot of nanotube conductance as the pH of PBS buffer is changed. A constant flow rate of 10 ml/hr is controlled by a syringe pump.

Figure 7 shows that the pH sensing signal takes 30 - 60 sec to develop when using a pressure-driven flow rate of 10 ml/hour. For slower flow rates (1 ml/hour) the signal settles in 100 - 200 sec. This lag time is also a function of the length and cross-section of piping in the microfluidics and the diffusion constant of the molecule being delivered to the sensor. Fast flow rates are desirable for minimizing the lead time, however, high flow rates use more sample volume and potentially create systematic sensing errors. For example, high flow rates are known to change the electrostatic potential at the sensor surface, thereby interfering with the sensing of charged proteins.[18]

The pH sensing experiment gives a lower limit of the lag-time for proteins to begin binding to a biosensor. Protons diffuse rapidly across flow lines and will reach the sensor surface faster than proteins. A spherical protein with a mass of 50 kDa has $D \sim 10^{-10}\,m^2s^{-1}$ (diffusion constants can easily be estimated from the Einstein relation $D = k_BT/6\pi\eta r$, where k_B is the Boltzman constant, T is temperature, η is the viscosity of water, and r is the protein radius which we estimate by assuming spherical geometry and protein density $1.2 \times 10^3\,kg/m^3$). Thus, the typical diffusion constant of a protein in solution is 100 times less than the diffusion constant of a proton in solution.

Figure 8 shows the effective change in gate voltage when pH is changed ΔV_g. The function $G(V_g)$ shown in Fig. 8a was used to convert $G(t)$ data from Figure 7 into $\Delta V_g(t)$. Changing the pH of the solution causes changes in the charge density at the SiO_2-water interface. When pH is increased to 9, the surface loses protons and ΔV_g is negative. When pH is decreased, the surface is protonated and ΔV_g is positive. These measurements are a useful calibration of the performance of the charge-sensitive biosensor. The theoretical maximum change in surface potential for SiO_2 is 60 mV/pH.[19] Figure 8b shows a change of roughly 40mV/pH, and we have observed a range of sensitivities from 10-50 mV/pH. Variability may be due to organic residues on the SiO_2 surface or variability in CNT diameters.
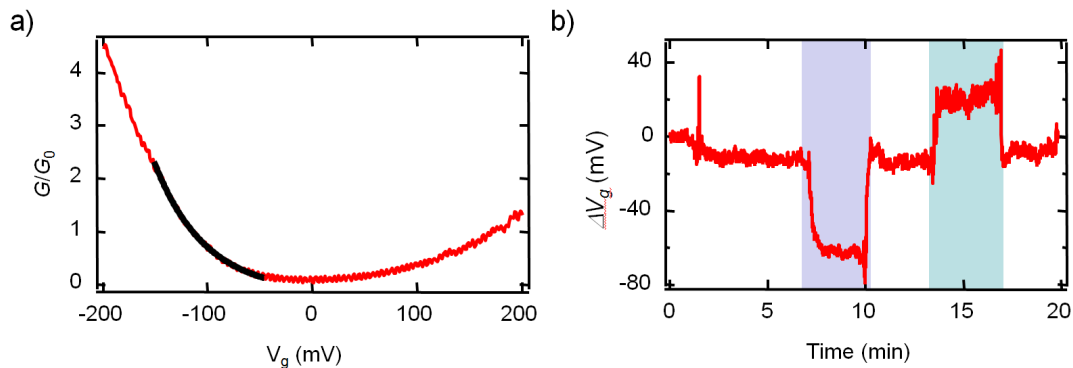

Figure 8 a) Transistor curve of the nanotube circuit from Figure 7, the black line is fit to the curve and is used to extrapolate the effective shift in gate voltage ΔV_g that is caused by changes in pH. The bulk solution potential V_g is set to -115 mV during the experiment. b) Plot of the shift in potential ΔV_g. The shift is zero at pH 7.4 and changes by 46mV when changing to pH 9, and changes by 36mV when changing to pH 6.

Temperature fluctuations can be a source of systematic error for nanoFET biosensor experiments. Changes in temperature can be introduced when warmer or cooler liquids are introduced to the microfluidic system. The most sensitive operating point of CNT-FET biosensor is the subthreshold region[8] where conductance is given by,[20]

$$G = G_o e^{-e(V_g - V_{th})/k_BT} \, ,\tag{1}$$

where e is the charge of an electron and V_{th} is the threshold gate voltage for the transistor to turn on. Equation 1 shows that device conductance depends exponentially on temperature.

Figure 9 illustrates how temperature sensitivity depends on V_g. At a typically operating point ($V_g - V_{th} = 200$ mV) conductance can swing by over 2% for a temperature change of 1°C. The issue of temperature control can be addressed by actively correcting temperature fluctuations using an on-chip temperature sensor and heater. An alternative, low-tech approach is to let all solutions equilibrate to room temperature before beginning a measurement.
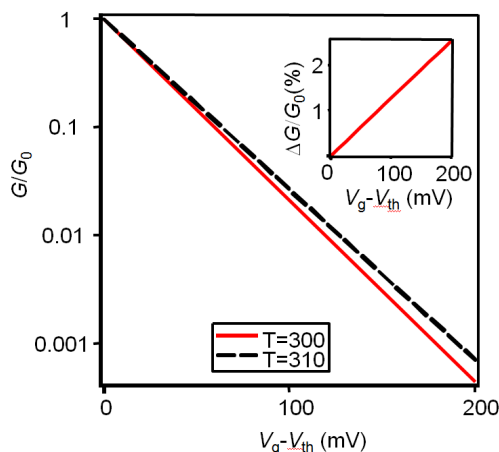

Figure 9. Temperature dependence of a CNT FET's conductance as a function of the difference between gate voltage V_g and the threshold voltage V_{th}. The insert shows the percent change in conductance for a temperature difference of 1°C.

4. FUNCTIONALIZATION OF NANOTUBES

In order to make a useful biological sensor, the surface of the sensor must bind the specific biomolecule of interest while rejecting other biomolecules. Specific binding of ss-dna can be achieved by using the complementary ss-dna. Specific binding of proteins can be achieved using antibodies or aptamers, as described below.

To functionalize the carbon nanotube we have followed a protocol developed by Chen et al.[21] Clean CNTs are incubated in a 1 mM solution of 1-pyrenebutanoic acid succinimidyl ester (PBASE, sold by Molecular Probes) in dimethylformamide (DMF). The incubation time is 5 hours. PBASE is chosen due to pyrene's ability to pi-stack on the CNT surface. The succinimidyl ester provides a handle for biomolecular conjugation. Succinimidyl ester is degraded by water and light, therefore, the DMF is dried of water using molecular sieves, and the solution is protected from light. After incubation, the chip is rinsed in dry DMF and then dried in nitrogen. A drop of 1mM ferritin in PBS was placed on the PBASE-functionalized CNTs and incubated for 3hrs. Ferritin was chosen because it is easy to image by atomic force microscopy and the primary amines on ferritin will conjugate to the succinimidyl ester. The resulting conjugation of ferritin to CNTs is shown in Figure 10. The scheme can easily be adapted to conjugate antibodies or aptamers to the CNT instead of ferritin.
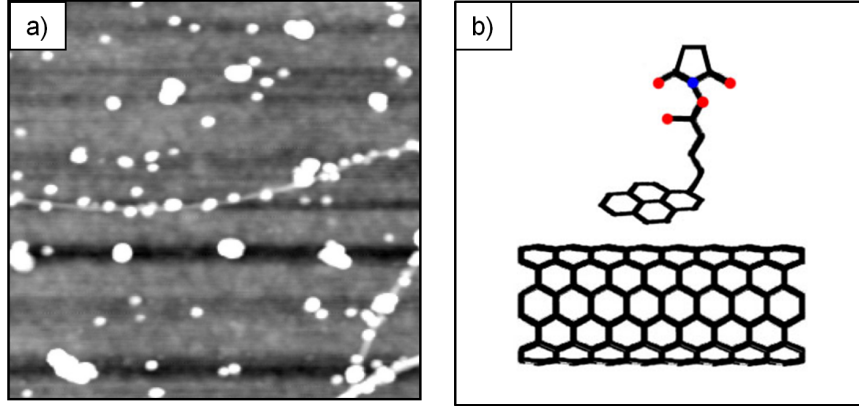
Figure 10. Conjugation of ferritin to CNTs. a) AFM image (1µmx1µm) of CNTs (white lines) that have been treated with PBASE and then ferritin (white dots). Some ferritin complexes stick specifically to the CNT, while others stick non-specifically to the silicon oxide surface. b) Schematic of the specific binding scheme. PBASE sticks to the side walls of the CNT by π stacking.

5. Electrostatic screening in solution

When a charged protein adsorbs to the surface of a CNT biosensor, the electrostatic coupling between the protein and the CNT depends on separation distance and counter-ion screening. Counter ion screening is characterized by the Debye screening length

$$\lambda_D = \frac{1\,\text{nm}}{\sqrt{c/93\,\text{mM}}} \tag{2}$$

where c is the monovalent salt concentration. The CNT biosensor response will decay exponentially with separation distance. The exponential decay constant is λ_D. To simulate biological conditions in our experiments we use phosphate buffered saline (PBS) with $\lambda_D \sim 1$ nm (137 mM NaCl and 10mM $Na_3(PO_4)$), therefore separation distances must be ~ 1 nm for optimal sensing.

Typical functionalization schemes utilize antibodies to specifically catch target biomolecules from solution. The antibody acts as 10-15 nm spacer between the CNT and the target biomolecule. Therefore, biosensing in biological conditions ($\lambda_D \sim 1$ nm) is not practical. Some authors have solved this issue by using low salt buffers.[22,23] Besides adding an additional sample preparation step, the use of low-salt buffers may reduce the affinity of antibody-antigen binding. Low salt concentrations can also lead to weak pH buffering (PBS is held at a stable pH by the buffering properties of phosphate ions). As shown in Fig. 7, fluctuations in pH will lead to large signals.

An alternative approach to the issue of electrostatic screening is to reducing the size of the functionalization molecule on the biosensor surface. Aptamers are a few nanometers in size and are a promising alternative to antibodies.[24]

7. ANALYZING SENSING DATA

Figure 11 shows two example sensing experiments that use biological molecules of different charge: polylysine (one positive charge per monomer at pH 7.4) and ss-dna (one negative charge per monomer at pH 7.4). From Figure 11 we see that polylysine binding is equivalent to a shift in gate voltage $\Delta V_g = +55$ mV. In other experiments we have observed a range 30 – 90 mV. From Figure 11 we see that ss-dna binding is equivalent to $\Delta V_g = -45$ mV.

We attribute sign of ΔV_g to the polarity of the biological molecules. Differences in the magnitude of ΔV_g are likely related to differences in binding geometry. Fluorescence imaging (not shown) reveals that polylysine binds to all bare silicon oxide surfaces. This binding is driven by the Coulomb interaction between negatively charged SiO2 (-2.5 μC/m^2 [25]) and positively charged polylysine. In contrast, previous studies of ss-dna show that the ss-dna only binds to the CNT and not the SiO$_2$.[26]
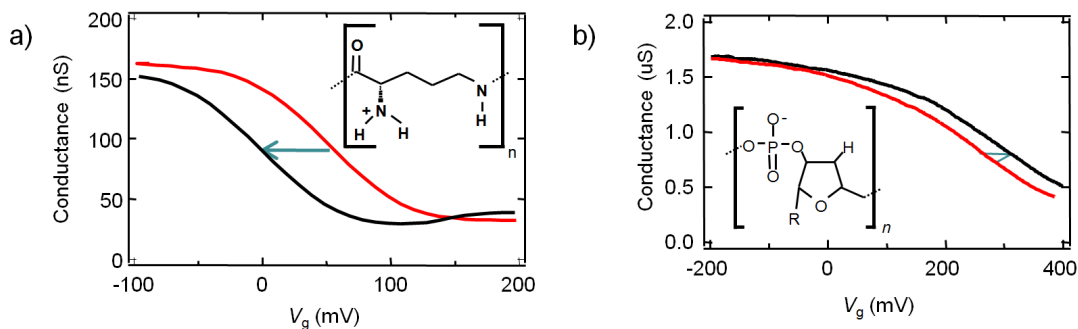
Figure 11. Biosensor signals depend on the charge of the biomolecule. a) Transistor curves measured before (red) and after (black) polylysine binding. The curve shifts 55 mV to the left, equivalent to ΔV_g = +55mV. b) Transistor curves measured before (red) and after (black) the binding of ss-dna. The curve shifts by about 45 mV to the right.

To compare ΔV_g due to polylysine binding to theoretical estimates we use the Gouy-Chapman Stern model. In this model, a layer of cations are bound to the negatively charged SiO$_2$ surface (this Stern layer is < 0.5 nm thick). A diffuse layer of additional screening ions extends into the solution. The diffuse layer can maintain a maximum potential difference of roughly $4k_BT$, or 100 mV.[27] Our CNTs range in diameter from 1 - 2 nm, therefore the majority of the CNT sits in the diffuse layer where ΔV_g is limited to 100 mV. This is consistent with our experiments where the highest measured shift for polylysine was 90 mV.

Figure 2b shows the real time binding of polylysine to a CNT sensor. The detection speed in this experiment is limited by the rate of protein binding which we can estimate using mass-transport theory as follows. In a simple model of protein flux we have, [28]

$$\delta = \left(\frac{DL}{\dot{\gamma}}\right)^{1/3} \quad , \tag{3}$$

$$Flux = \frac{DC_o}{\delta} \quad , \tag{4}$$

where δ is the depletion length, γ is the shear rate, L is the length of the binding region, and C_o is the original concentration proteins in solution. For the experiment shown in Fig. 2b, L = 1.4mm, γ = 27 s^{-1}, C_o = 90 nM, and D = 4 x 10^{-13} m^{2}s^{-1}.[29] Using equations 3 and 4 we can calculate a flux of 8x10^{12} m^{-2}s^{-1}.

To compare this above theoretical prediction to observed protein flux, we consider the time for the signal to saturate. Figure 2b shows a clear signal saturation after approximately 1.5 minutes. This saturation occurs when accumulated polylysine neutralizes the charged SiO$_2$ surface (the bare charge of SiO$_2$ is -2.5 μC/cm^2 or roughly $-e$ per 6 nm^2, where e is the charge of the electron) [25]. Since each polylysine molecule carries a charge of +800e, the predicted flux of 8x10^{12} m^{-2}s^{-1} will lead to charge neutrality after 26 s, faster than the time for fully developed flow (Fig. 7). Therefore, the observed 1.5 min saturation time is consistent with theoretical predictions for mass transport.

Based on this simple mass-transport theory, and the signal-to-noise ratio in our CNT FET biosensors, we can estimate the lowest concentration of polylysine that is compatible with rapid detection. When polylysine binding reaches 20% saturation the signal is well above the noise level (Figure 2b). We arbitrarily define rapid detection as 5 minutes. Using other sensor parameters described above, we conclude that the lower limit for rapid detection is 8 nM. We are currently seeking ways to decrease this lower limit, to access the picomolar concentrations that are most relevant for medical diagnostics.

[1]Homola, J. "Present and future of surface plasmon resonance biosensors" Analytical and Bioanalytical Chemistry *377*, 528 (2003).

[2]Yan, R.,Mestas, S.,Yuan, G.,Safaisini, R.,Dandy, D. Lear, K. "Label-free silicon photonic biosensor system with integrated detector array" Lab on a Chip *9*, 2163 (2009).

[3]Daniels, Jonathan S. Pourmand, N. "Label-Free Impedance Biosensors: Opportunities and Challenges" Electroanalysis *19*, 1239 (2007).

[4]Waggoner, P. S. Craighead, H. G. "Micro- and nanomechanical sensors for environmental, chemical, and biological detection" Lab on a Chip *7*, 1238 (2007).

[5]Patolsky, F.,Zheng, G. Lieber, C. M. "Nanowire-Based Biosensors" Analytical Chemistry *78*, 4260 (2006).

[6]Allen, B. L.,Kichambare, P. D. Star, A. "Carbon Nanotube Field-Effect-Transistor-Based Biosensors" Advanced Materials *19*, 1439 (2007).

[7]Heath, J. R.,Davis, M. E. Hood, L. "Nanomedicine-Revolutionizing the Fight against Cancer" Scientific American, (2009).

[8]Heller, I.,Janssens, A. M.,Mannik, J.,Minot, E. D.,Lemay, S. G. Dekker, C. "Identifying the Mechanism of Biosensing with Carbon Nanotube Transistors" Nano Letters *8*, 591 (2007).

[9]Kong, J.,Soh, H. T.,Cassell, A. M.,Quate, C. F. Dai, H. "Synthesis of individual single-walled carbon nanotubes on patterned silicon wafers" Nature *395*, 878 (1998).

[10]Kang, S. J.,Kocabas, C.,Ozel, T.,Shim, M.,Pimparkar, N.,Alam, M. A.,Rotkin, S. V. Rogers, J. A. "High-performance electronics using dense, perfectly aligned arrays of single-walled carbon nanotubes" Nat Nano *2*, 230 (2007).

[11]Wang, C.,Zhang, J.,Ryu, K.,Badmaev, A.,De Arco, L. G. Zhou, C. "Wafer-Scale Fabrication of Separated Carbon Nanotube Thin-Film Transistors for Display Applications" Nano Letters *9*, 4285 (2009).

[12]Ding, L.,Yuan, D. Liu, J. "Growth of High-Density Parallel Arrays of Long Single-Walled Carbon Nanotubes on Quartz Substrates" Journal of the American Chemical Society *130*, 5428 (2008).

[13]Ding, L.,Tselev, A.,Wang, J.,Yuan, D.,Chu, H.,McNicholas, T. P.,Li, Y. Liu, J. "Selective Growth of Well-Aligned Semiconducting Single-Walled Carbon Nanotubes" Nano Letters *9*, 800 (2009).

[14]Ishigami, M.,Chen, J. H.,Cullen, W. G.,Fuhrer, M. S. Williams, E. D. "Atomic Structure of Graphene on SiO2" Nano Letters *7*, 1643 (2007).

[15]Zhu, J.,Brink, M. McEuen, P. L. "Single-Electron Force Readout of Nanoparticle Electrometers Attached to Carbon Nanotubes" Nano Letters *8*, 2399 (2008).

[16]Duffy, D. C.,McDonald, J. C.,Schueller, O. J. A. Whitesides, G. M. "Rapid Prototyping of Microfluidic Systems in Poly(dimethylsiloxane)" Analytical Chemistry *70*, 4974 (1998).

[17]Minot, E.,Janssens, A.,Heller, I.,Heering, H.,Dekker, C. Lemay, S. "Carbon nanotube biosensors: The critical role of the reference electrode" Applied Physics Letters *91*, 093507 (2007).

[18]Bourlon, B.,Wong, J.,Miko, C.,Forro, L. Bockrath, M. "A nanoscale probe for fluidic and ionic transport" Nat Nano *2*, 104 (2007).

[19]Hal van, R. E. G.,Eijkel, J. C. T. Bergveld, P. "A novel description of ISFET sensitivity with the buffer capacity and double-layer capacitance as key parameters" Sensors and Actuators B: Chemical *24-25*, 201 (1995).

[20]Rosenblatt, S.,Yaish, Y.,Park, J.,Gore, J.,Sazonova, V. McEuen, P. L. "High Performance Electrolyte Gated Carbon Nanotube Transistors" Nano Letters *2*, 869 (2002).

[21]Chen, R. J.,Zhang, Y.,Wang, D. Dai, H. "Noncovalent Sidewall Functionalization of Single-Walled Carbon Nanotubes for Protein Immobilization" Journal of the American Chemical Society *123*, 3838 (2001).

[22]Stern, E.,Wagner, R.,Sigworth, F. J.,Breaker, R.,Fahmy, T. M. Reed, M. A. "Importance of the Debye Screening Length on Nanowire Field Effect Transistor Sensors" Nano Letters *7*, 3405 (2007).

[23]Zheng, G.,Patolsky, F.,Cui, Y.,Wang, W. U. Lieber, C. M. "Multiplexed electrical detection of cancer markers with nanowire sensor arrays" Nat Biotech *23*, 1294 (2005).

[24]Maehashi, K.,Katsura, T.,Kerman, K.,Takamura, Y.,Matsumoto, K. Tamiya, E. "Label-Free Protein Biosensor Based on Aptamer-Modified Carbon Nanotube Field-Effect Transistors" Analytical Chemistry *79*, 782 (2006).

[25]Artyukhin, A. B.,Stadermann, M.,Friddle, R. W.,Stroeve, P.,Bakajin, O. Noy, A. "Controlled Electrostatic Gating of Carbon Nanotube FET Devices" Nano Letters *6*, 2080 (2006).

[26]Star, A.,Tu, E.,Niemann, J.,Gabriel, J.,Joiner, C. Valcke, C. "Label-free detection of DNA hybridization using carbon nanotube network field-effect transistors" Proceedings of the National Academy of Sciences of the United States of America *103*, 921 (2006).

[27]Bard, A. J. Faulkner, L., [*ELECTROCHEMICAL METHODS Fundamentals and Apllications*], John Wiley& Sons, (2001).

[28]Squires, T. M.,Messinger, R. J. Manalis, S. R. "Making it stick: convection, reaction and diffusion in surface-based biosensors" Nat Biotech *26*, 417 (2008).

[29]Rodriguez-Maldonado, L.,Fernandez-Nieves, A. Fernández-Barbero, A. "Dynamic light scattering from high molecular weight poly-l-lysine molecules" Colloids and Surfaces A: Physicochemical and Engineering Aspects *270*, 335 (2005).